JVST B
Journal of Vacuum Science & Technology B

ARTICLE

avs.scitation.org/journal/jvb

3D modeling of electron-beam lithographic process from scanning electron microscope images

Cite as: J. Vac. Sci. Technol. B **39**, 012603 (2021); doi: 10.1116/6.0000694
Submitted: 6 October 2020 · Accepted: 29 December 2020 ·
Published Online: 19 January 2021

View Online

Export Citation

CrossMark

Dehua Li,[1] Soo-Young Lee,[1,a)] Jin Choi,[2] Seom-Beom Kim,[2] and Chan-Uk Jeon[2]

AFFILIATIONS

[1]Department of Electrical and Computer Engineering, Auburn University, Auburn, Alabama 36849
[2]Samsung Electronics, Mask Development Team, 16 Banwol-Dong, Hwasung, Kyunggi-Do 445-701, Korea

[a)]**Author to whom correspondence should be addressed:** leesooy@eng.auburn.edu

ABSTRACT

Computational lithography is typically based on a model representing the lithographic process where a typical model consists of three components, i.e., line spread function, conversion formula (exposure-to-developing rate conversion), and noise process (exposure fluctuation). In our previous study, a practical approach to modeling the e-beam lithographic process by deriving the three components directly from SEM images was proposed. However, a 2D model of a substrate system was employed; i.e., the exposure variation along the resist-depth dimension was not considered. In this study, the possibility of improving the accuracy of modeling using a 3D model is investigated. The 3D model is iteratively determined by modeling the critical dimension estimated based on the model to those measured in SEM images. This paper describes the 3D modeling approach and new optimization procedures and discusses in detail the results from an extensive simulation for an accuracy analysis of the 3D modeling approach.

Published under license by AVS. https://doi.org/10.1116/6.0000694

I. INTRODUCTION

Electron-beam (e-beam) lithography is widely employed in the pattern transfer onto a resist.[1–6] The high fidelity of e-beam lithography plays a very important role in a variety of applications, such as fabrication of photo-masks, prototype devices, small volume production for custom circuits, etc. However, two of the main issues that limit the minimum feature size and the maximum feature density achievable by e-beam lithography are the proximity effect and line edge roughness (LER).[7] The proximity effect in e-beam lithography is caused by the electron scattering and makes the written feature blurred limiting the spatial resolution in a circuit pattern. Also, the LER is mainly due to the stochastic processes involved in the e-beam exposing and resist-development steps. Various methods have been developed in order to correct the proximity effect and reduce the LER, employing analytic, simulation, or experimental approaches.[8–11] In the computational lithography, such efforts are based on a model representing the lithographic process where a typical model consists of three components, i.e., the point spread function (PSF, equivalent to the line spread function, LSF), conversion formula (exposure-to-developing rate conversion), and noise process (exposure fluctuation).

In our previous study,[12] a practical approach to modeling the e-beam lithographic process by deriving the three components directly from the scanning electron microscope (SEM) images was proposed. Based on the critical information extracted from SEM images, the modeling process derives the three components through iterations. However, a two-dimensional (2D) model was employed; i.e., the exposure variation along the resist-depth dimension was not considered. Since the dependency of the exposure energy deposited on the resist layer is ignored, such a modeling approach is likely to lead to inaccurate results, especially for a thick resist or a low beam energy.

This study attempts to improve the modeling accuracy by taking into account the exposure dependency on the resist layer, i.e., a three-dimensional (3D) modeling approach. A 3D model enables a more realistic representation of exposure distribution in the resist and in turn allows one to obtain a more accurate remaining resist profile through the resist-development simulation.[13] Therefore, it is more likely to derive a more realistic model of an e-beam lithographic process by the 3D approach. Also, the modeling procedures are simplified and optimized in order to reduce the computational complexity without sacrificing the accuracy of modeling. Through an extensive simulation with reference to remaining

Published under license by AVS.

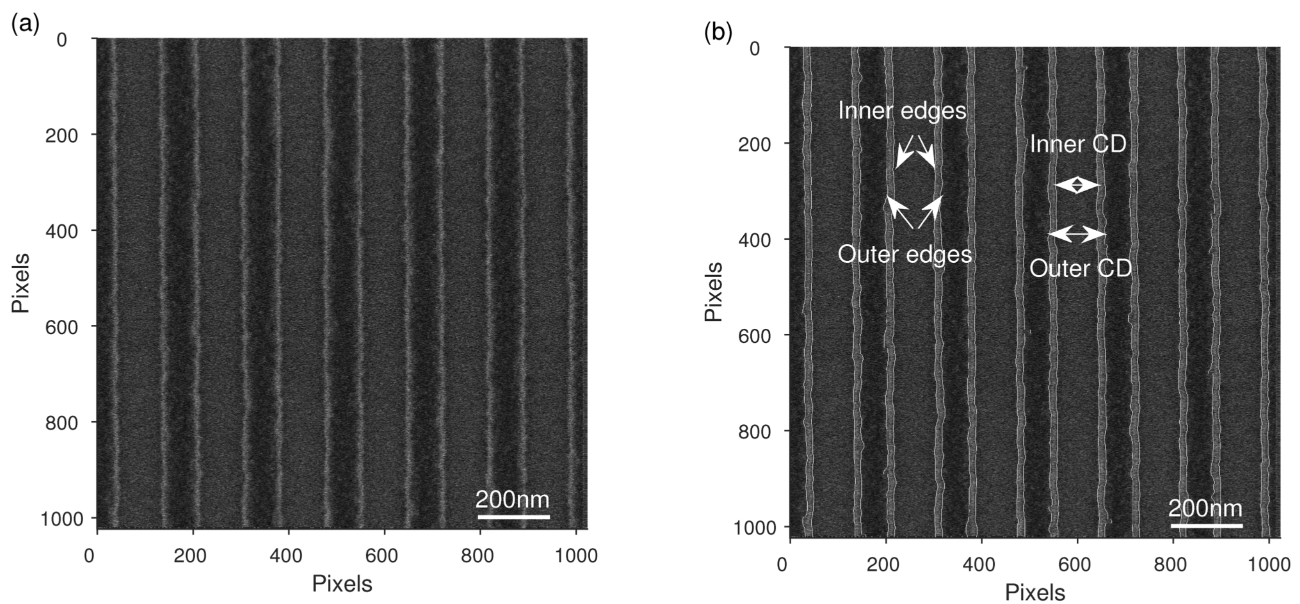

FIG. 1. (a) Example of an SEM image in a L/S pattern and (b) detected boundaries overlapped on an SEM image in (a). The inner and outer edges are used to calculate the CD and LER.

resist profiles, it has been shown that the 3D modeling can achieve a higher accuracy, i.e., a smaller modeling error of critical dimension (CD) in line/space (L/S) patterns, compared to the 2D approach. The modeling result is further verified through the proximity effect correction by the dose control.

The rest of the paper is organized as follows. The 2D modeling approach is reviewed in Sec. II. The 3D modeling approach is described in Sec. III, and the dose correction is described in Sec. IV. The modeling and verification results are discussed in Sec. V, followed by a summary in Sec. VI.

II. 2D MODELING APPROACH

In our previous study,[12] a 2D resist model was employed in modeling the e-beam lithographic process; i.e., the exposure variation along the resist-depth dimension was not taken into account. The three components of the e-beam lithographic process are modeled through iterations by minimizing the modeling error, which consists of the modeling errors of the CD and LER. The CD modeling error is defined as the difference between the modeled CD and the CD measured in SEM images and the LER modeling error as the difference between the modeled and the measured LERs. An example of an SEM image with the detected edges is shown in Fig. 1. The CD and LER are measured from the detected inner and outer edges of a feature. In order to make the convergence easier to achieve, the 2D modeling is carried out in two steps, i.e., the line-width (or CD) matching followed by the LER matching.

The deterministic LSF instead of the PSF is modeled since L/S patterns are considered. In each iteration, the exposure distribution is computed from the stochastic LSF and converted into the developing rate. Then, the remaining resist profile is obtained from the exposure distribution through the development simulation using the path-based method.[13] From the remaining resist profile, the CD and LER are computed from the feature boundaries. Then, the model is adjusted such that the modeling error is reduced.

The effectiveness of the 2D modeling approach was well demonstrated for the case of relatively thin resist and high beam energy in the previous study. However, this modeling relies on a 2D model; i.e., the exposure variation along the resist-depth dimension is not considered. Therefore, when the exposure variation among layers in a resist is significant, such as for a thicker resist, the 2D modeling approach can lead to significant errors in modeling the e-beam lithographic process. In order to reduce the modeling error, a more realistic model needs to be employed. Hence, in the new approach, a 3D model of a resist layer is adopted and the modeling procedures are also improved.

The improved procedures are applicable to the 2D approach too. In comparison with the 3D approach in Sec. V, the improved 2D approach will be referred to.

III. 3D MODELING APPROACH

In the proposed modeling approach, a 3D resist model of five layers (see Fig. 2) is employed so that the exposure variation along the depth dimension of resist is taken into account in order to enhance the accuracy and applicability of modeling. An overview of the approach is presented first, and then the models and procedures involved in the modeling process are described in detail.

Published under license by AVS.

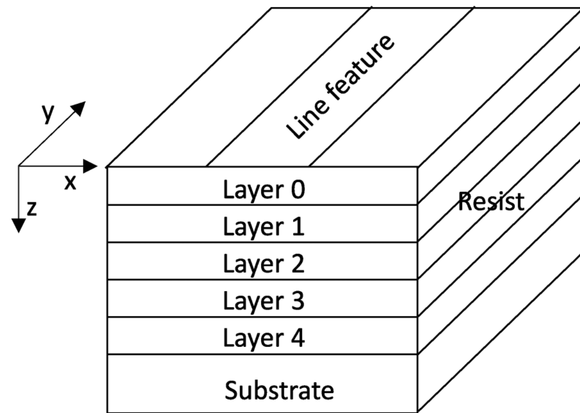

FIG. 2. Resist model includes five resist layers, where the middle layer of the resist is taken as the reference layer for the purpose of the 3D modeling.

A. Overview

The goal of the modeling is to derive the LSF and noise models from experimental results such that the models can be used in the estimation and optimization for the same e-beam lithographic process. The noise represents the stochastic fluctuation of exposure. Through an iterative procedure, the LSF and noise are modeled, being guided by CD measurements obtained from SEM images. In order to keep the complexity of modeling low, the conversion formula is fixed. The overall flow of the modeling process is depicted in Fig. 3.

A set of parameters is used in representing each of LSF and noise models, and the iterative modeling process is structured following the simulated annealing (SA) procedure. In each iteration, (i) the model parameters are randomly perturbed (adjusted), (ii) the exposure distribution (of each of the circuit patterns from which the CD measurements are taken) is computed using the adjusted LSF and noise models, (iii) from the exposure distribution, the remaining resist profile is obtained through a resist-development simulation, and (iv) the CD is measured from the remaining resist profile and the CD modeling error is computed. The steps from (i) to (iv) are repeated for each of the CD measurements from SEM images. The change in the total CD modeling error, i.e., cost function, determines the probability of accepting the adjusted models of LSF and noise. The iteration continues until an acceptable modeling error is achieved.

B. Exposure distribution

In Fig. 4, the deterministic exposure distribution for a single line is plotted for five layers, where the variation of the exposure distribution along the resist-depth dimension can be clearly seen.

Since L/S patterns are considered in this study, the LSF, instead of PSF, is employed to facilitate the modeling process. The stochastic LSF can be represented by the corresponding deterministic LSF, denoted by $lsf_d(x, z)$, to which the noise is added. Therefore, the deterministic LSF and noise are modeled. Modeling

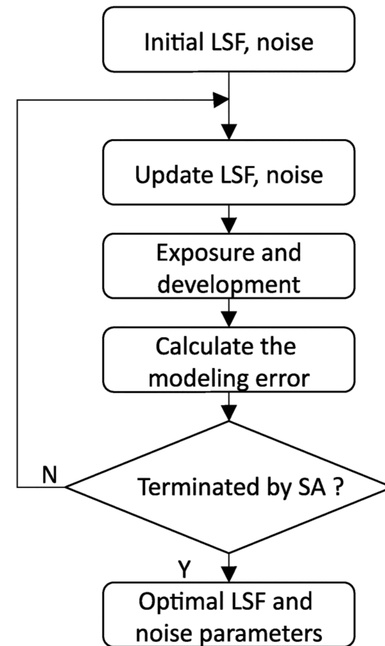

FIG. 3. Overall flow of the modeling approach: the modeling is guided by simulate annealing.

the deterministic LSFs of five layers independently would require a high complexity of computation and may not guarantee the convergence of modeling. To reduce the complexity, the LSF at a reference layer is modeled and the LSFs at other layers are derived from the LSF at the reference layer. This derivation is guided by the layer-dependency ratio, $LR(x, z)$, defined as follows:

$$LR(x, z) = \frac{lsf_d(x, z)}{lsf_d(x, z_0)}, \tag{1}$$

where $lsf_d(x, z)$ and $lsf_d(x, z_0)$ are the deterministic LSFs at a layer and the reference layer, respectively.

A number of instances of stochastic LSF are generated from a Monte Carlo simulation (CASINO) and then the deterministic LSF for each layer is obtained by averaging the instances for the layer.[14] Then, the LR can be computed from the deterministic LSFs. In Fig. 5, an example of the LR obtained using the CASINO software is provided. In the modeling, the stochastic LSF at a layer other than the reference layer is computed as follows:

$$lsf(x, z) = lsf(x, z_0) \cdot LR(x, z). \tag{2}$$

C. Noise model

The noise, i.e., exposure fluctuation, tends to have the following characteristics: when the exposure level, i.e., deterministic

Published under license by AVS.

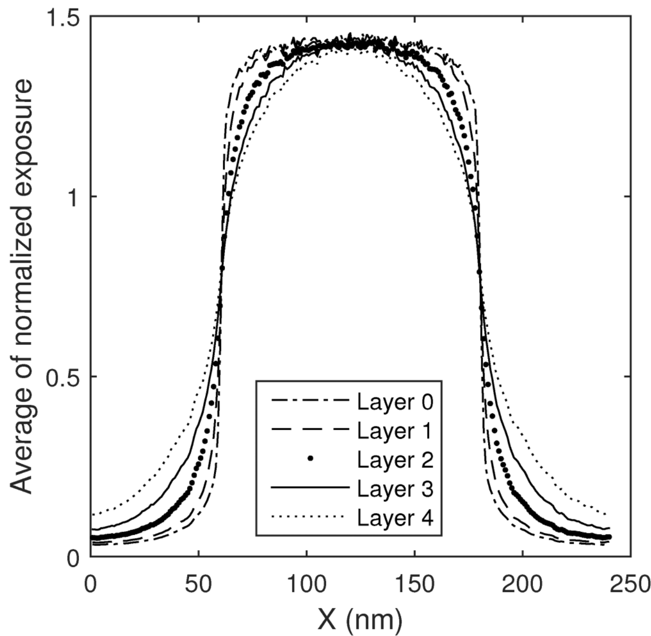

FIG. 4. Example of an average exposure distribution along the Y direction at different layers from the PMMA/Si system: a linewidth of 120 nm, a resist thickness of 300 nm, and a beam energy of 10 keV. The average exposure varies along the resist-depth dimension.

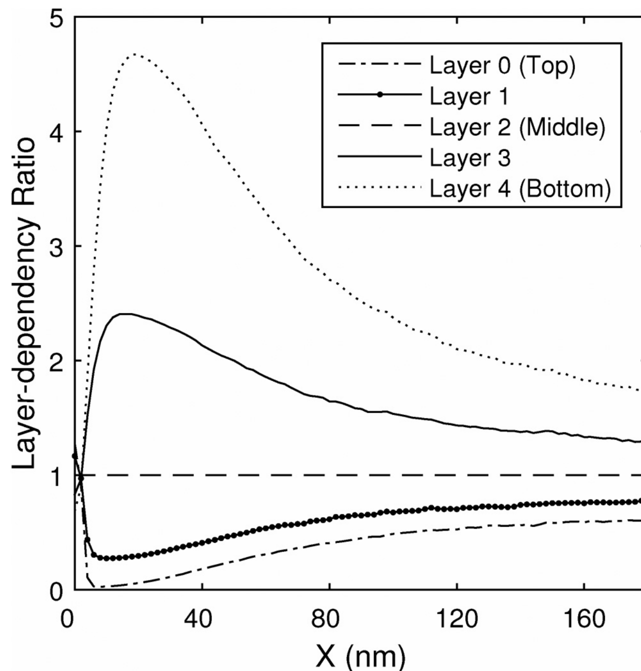

FIG. 5. Example of a layer-dependency ratio: a resist thickness of 200 nm and a beam energy of 30 keV in the PMMA/Si system.

exposure, is higher, the absolute fluctuation of exposure is larger, while the relative fluctuation, defined as the absolute fluctuation normalized to the average (deterministic) exposure, is smaller.[12] Note that the deterministic exposure is highest at the center ($x = 0$) of LSF. The noise, $e_n(x)$, at the reference layer ($z = z_0$) is modeled as follows:

$$e_n(x) = rand \cdot \sigma_0 \left(\frac{lsf_d(x, z_0)}{lsf_d(0, z_0)} \right)^{\alpha}, \tag{3}$$

where $rand$ is a random number of the normal distribution $N(0, 1)$, σ_0 is a noise level at the center of LSF, and α is a parameter ($0 < \alpha < 1$).

Through iterations, σ_0 and α are to be estimated. Then, the stochastic exposure at the reference layer is calculated as

$$lsf(x, z_0) = lsf_d(x, z_0) + e_n(x). \tag{4}$$

To facilitate the modeling process, certain constraints to be imposed on the noise model are derived from the data obtained by a Monte Carlo simulation. The σ_0 must be within 2–18% of the exposure level at the center (peak) of LSF and α in the range of 0.3–0.7.

D. LSF model

The computation of the 3D distribution of stochastic exposure starts from the deterministic LSF at the reference layer as described above. In this study, the middle layer of resist is used as the reference layer. Therefore, the deterministic LSF at the middle layer is modeled. Since an LSF is symmetric with respect to its center ($x = 0$), only one side ($x \geq 0$) needs to be considered in the modeling.

In the previous study,[12] the LSF was modeled point-by-point, which resulted in a high complexity of modeling and made the convergence hard to achieve. In this study, the characteristics of LSF are utilized to lower the complexity and also enable an easier convergence. A typical LSF monotonically decreases as the distance, x, from the center increases. It varies (decreases) fast where x is relatively small and very slow beyond a point, to be referred to as a turning point. Therefore, the deterministic LSF can be represented by two parts, i.e., the fast-varying ("main lobe") and slow-varying ("tail") parts where the two parts are connected through the turning point as illustrated in Fig. 6. The main lobe is modeled point-by-point for sufficient flexibility. On the other hand, the tail is modeled by an exponential function as in Eq. (5), which involves only three parameters,

$$lsf_d(x, z_0) = V_t \cdot b^{(x - x_t)}, \tag{5}$$

where V_t is the deterministic exposure at the turning point, x_t is the turning point, and b is the base of the exponential function ($b < 1$).

Since the domain of the main lobe is much smaller than that of tail, the reduction of complexity is significant.

Published under license by AVS.

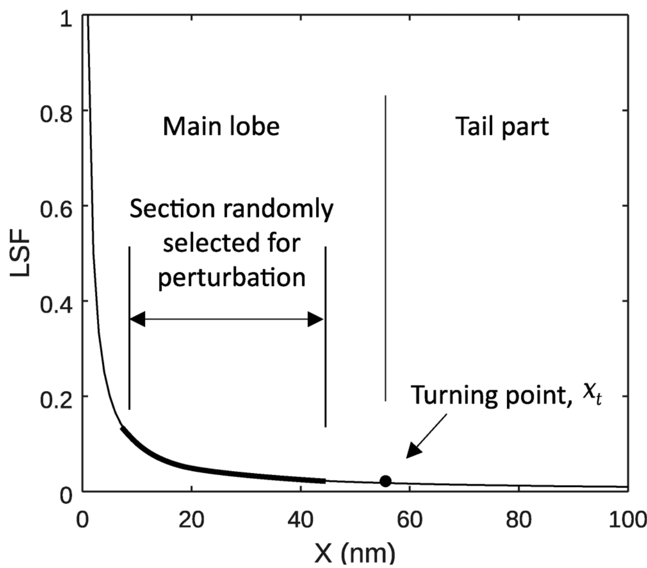

FIG. 6. Illustration of LSF adjustment: In an iteration, the length, location, and scaling of the perturbed section in the main lobe are randomly determined.

In order to facilitate the modeling process and achieve a convergence to an acceptable LSF, a few constraints, obtained from a Monte Carlo simulation, are imposed on the LSF, including the shape of the main lobe (80–180% of the simulated LSF), the location of the turning point (3–100 nm), the base b (0.96–0.99), and the ratio of the peak to the next point (<1.25).

E. Cost function

The cost function quantifies a modeling error and the iterative modeling process continues until the (value of) cost function is reduced below an acceptable threshold. In the previous study,[12] both CD and LER modeling errors were included in the cost function. However, the LER modeling error is excluded from the cost function in this study to enable a lower complexity of modeling, leading to a faster and more stable convergence. The exposure fluctuation (noise), which causes the LER, affects the CD; i.e., a higher level of fluctuation makes the CD larger. Therefore, this new cost function takes into account the effect of noise and, therefore, can be considered to reflect the LER modeling error indirectly.

The CD modeling error is defined as the difference between the modeled and reference CDs at a layer where the reference CD is defined as the CD measured in the reference remaining resist profile. In the previous study, the CD modeling error was computed using the average of the top and bottom CDs, i.e., the average of CDs at the top and bottom layers of resist. In order to obtain a more realistic modeling result, the CD modeling error is evaluated at each of the top and bottom layers. The cost function ϵ is defined as the average modeling error,

$$\epsilon = \frac{1}{N}\sum_{i=1}^{N}|CD_{m,i} - CD_{ref,i}|, \tag{6}$$

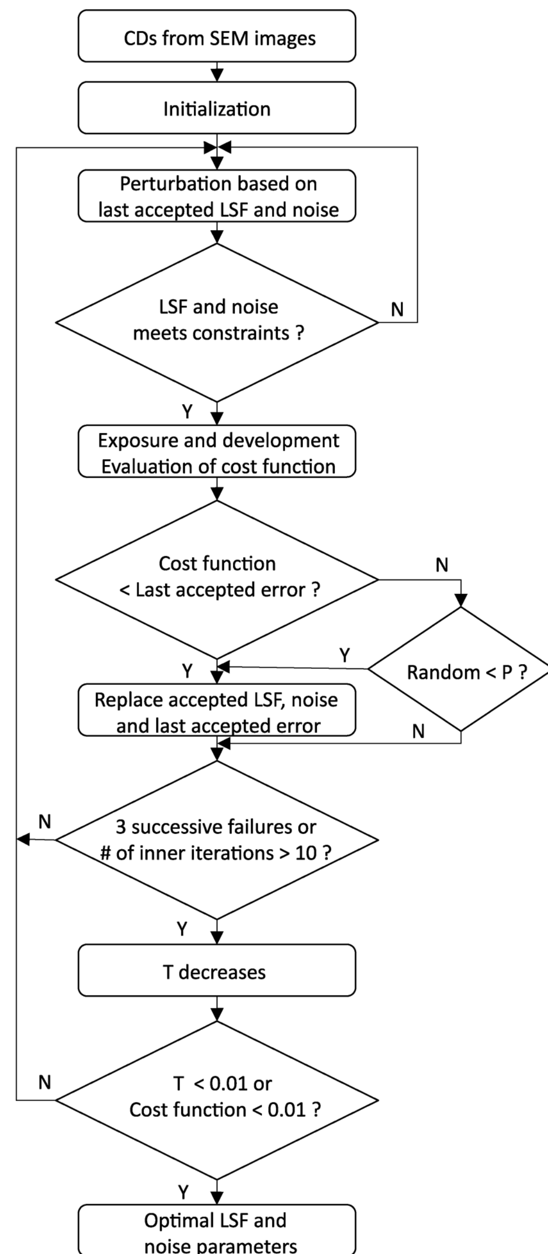

FIG. 7. Linewidth matching guided by SA is employed in the modeling process to minimize the cost function. In each iteration, the perturbed LSF and noise parameters are utilized going through the exposure and resist-development processes in order to compute the cost function.

Published under license by AVS.

where $CD_{m,i}$ and $CD_{ref,i}$ are the ith modeled and reference CDs, respectively, and N is the total number of the top and bottom CDs from the SEM images.

F. Simulated annealing

The iterative modeling process is guided by the simulated annealing, and the flow of modeling is shown in Fig. 7. The modeling process consists of outer and inner loops. The outer loop corresponds to the annealing temperature. The inner loop is finished after three successive perturbations are rejected or iterated up to ten times to allow sufficient annealing. In each iteration, the deterministic LSF and noise are randomly perturbed. The stochastic exposure distribution is computed using the stochastic LSF derived from the perturbed deterministic LSF and noise. Through the resist-development simulation, the remaining resist profile is obtained, from which the modeled CD and subsequently the CD modeling error are computed. This process is repeated for each measurement of CD. Then, the cost function is evaluated, and the probability P of accepting the perturbed deterministic LSF and noise is computed as

$$P = \min\left\{1,\ e^{-\frac{\epsilon_c - \epsilon_a}{T}}\right\}, \tag{7}$$

where ϵ_c is the modeling error (cost function) in the current iteration, ϵ_a is the last accepted modeling error, and T is the annealing temperature.

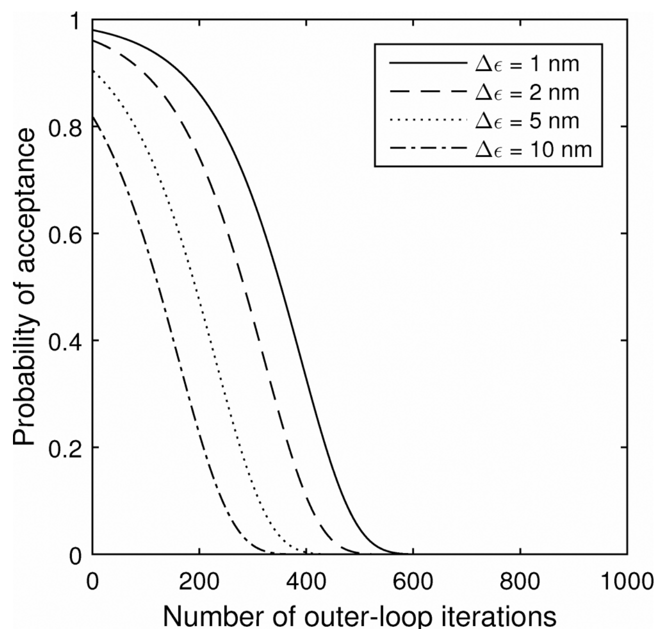

FIG. 8. Probability of acceptance decreases as the number of outer-loop iterations increases (corresponding to the decrease of annealing temperature) for $\Delta\epsilon > 0$.

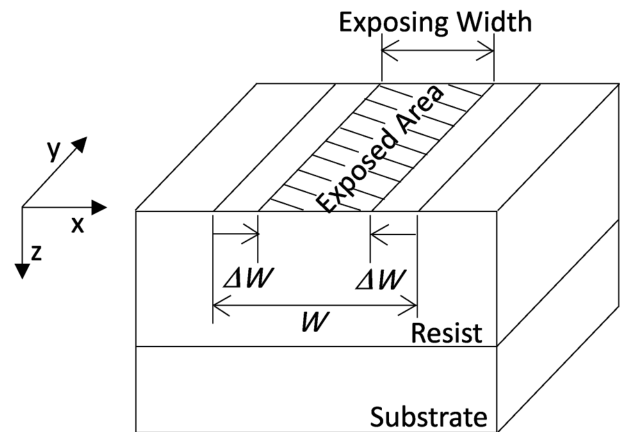

FIG. 9. Feature width is reduced by ΔW on each side and the dose is determined for the reduced width.

The behavior of P (for $\Delta\epsilon > 0$) is plotted in Fig. 8, where $\Delta\epsilon = \epsilon_c - \epsilon_a$. The perturbed deterministic LSF and noise are accepted with the probability of P. This annealing process is continued until the cost function goes below a threshold (0.01 nm) or

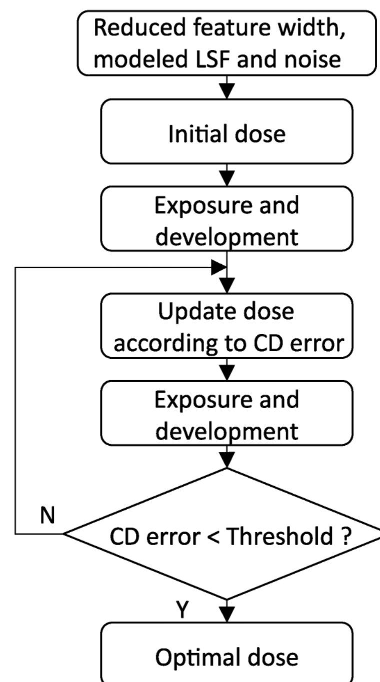

FIG. 10. Optimal dose is determined when the CD error (calculated with the modeled LSF, noise parameters, and the reduced feature linewidth to be exposed) is below a threshold, which is set to a small value.

Published under license by AVS.

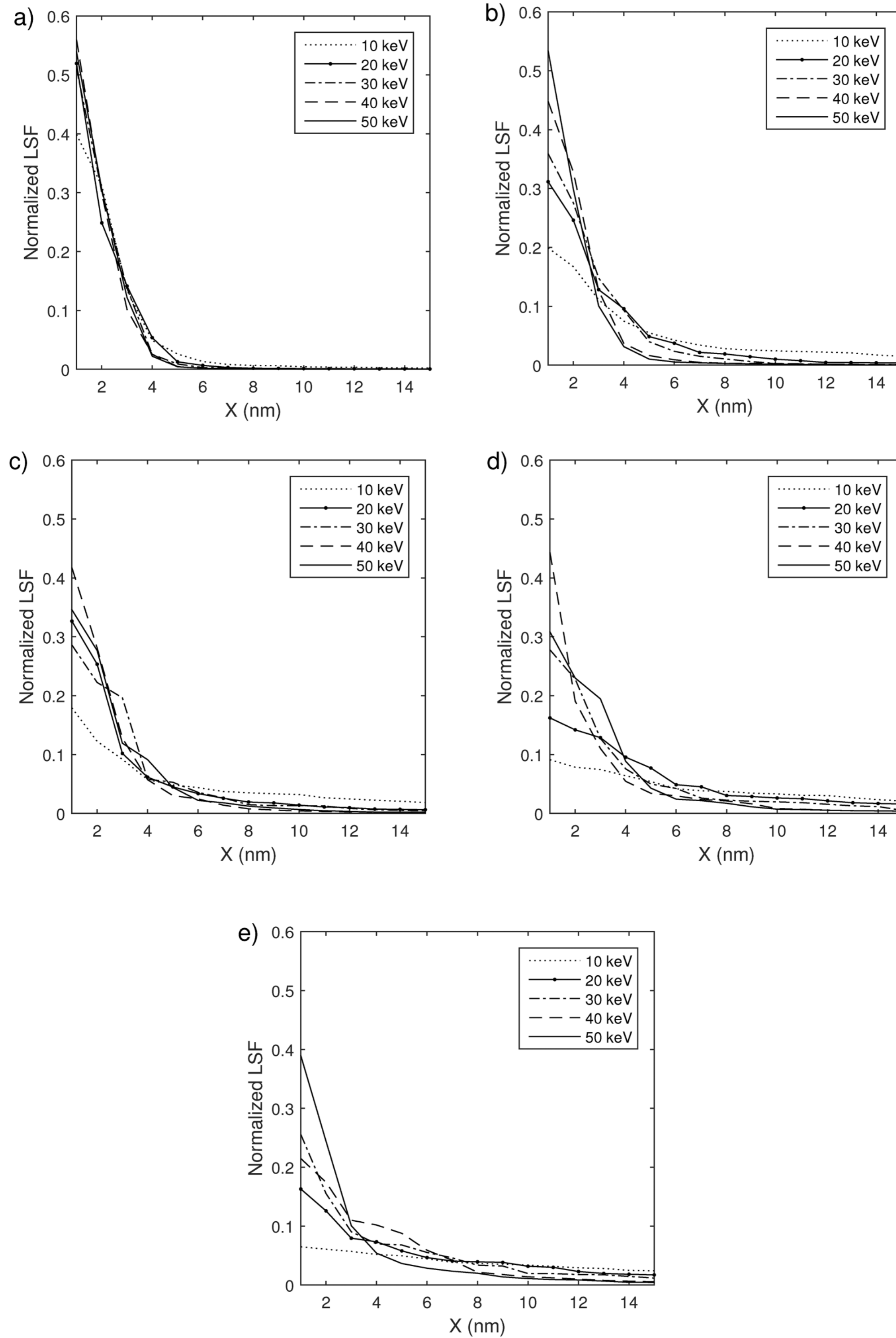

FIG. 11. Deterministic LSFs from the 3D modeling procedures for varying beam energy from 10 to 50 keV and resist thicknesses of (a) 100 nm, (b) 200 nm, (c) 300 nm, (d) 400 nm, and (e) 500 nm.

Published under license by AVS.

the maximum number of iterations allowed (or $T < 0.01$) is reached.

G. Initialization

The deterministic LSF and noise are initialized subject to the respective constraints (refer to Secs. III C and III D): The initial deterministic LSF for the iterative modeling process is obtained by randomly changing the LSF, up to 20%, used in generating the corresponding reference resist profiles. The location of turning point x_t is initialized to the location where the value of LSF is 1% of the peak, the base b to 0.97, σ_0 to 8% of the peak of LSF, and α to 0.5.

H. Perturbation

In each iteration, the deterministic LSF and noise are randomly perturbed with the following guidelines.

A selected section of the main lobe is scaled up or down where the location S ($0 \le S < x_t$) and length L ($1 \le L \le 8$ nm) of the section are randomly decided. The perturbation ranges of the scaling factor for the selected section of LSF, the base b of the exponential function for the tail part, the noise level σ_0, and α for the noise are reduced from 150% (in the early stage) to 2% (in the final stage) of the allowed ranges mentioned in Sec. III D through iterations. The location x_t of the turning point is changed up to ± 1 nm in each iteration.

TABLE I. Results from 2D and 3D modeling with resist thickness varied from 100 to 300 nm and beam energy from 10 to 50 keV.

Thickness (nm)	Beam energy (keV)	3D/2D	Modeling error (nm/layer)	σ_0	α	x_t (nm)	b
100	10	3D	0.33	0.0037	0.517	35	0.965
		2D	2.57	0.0070	0.519	20	0.977
	20	3D	0.37	0.0038	0.532	46	0.971
		2D	1.07	0.0025	0.543	28	0.970
	30	3D	0.11	0.0023	0.463	91	0.976
		2D	0.59	0.0018	0.484	18	0.978
	40	3D	0.06	0.0046	0.505	14	0.961
		2D	0.41	0.0013	0.518	37	0.965
	50	3D	0.09	0.0083	0.522	21	0.970
		2D	0.30	0.0013	0.488	90	0.971
200	10	3D	2.74	0.0288	0.519	18	0.961
		2D	8.66	0.0203	0.533	56	0.970
	20	3D	0.97	0.0195	0.520	29	0.969
		2D	5.41	0.0064	0.535	82	0.985
	30	3D	0.53	0.0053	0.544	26	0.966
		2D	3.02	0.0057	0.521	76	0.967
	40	3D	0.17	0.0054	0.526	22	0.970
		2D	2.37	0.0052	0.497	33	0.973
	50	3D	0.12	0.0020	0.507	86	0.988
		2D	1.57	0.0023	0.491	24	0.964
300	10	3D	1.14	0.0133	0.534	64	0.962
		2D	16.99	0.0138	0.465	79	0.966
	20	3D	0.34	0.0132	0.560	58	0.964
		2D	9.21	0.0106	0.554	83	0.987
	30	3D	0.94	0.0091	0.505	34	0.974
		2D	7.43	0.0108	0.462	40	0.965
	40	3D	0.14	0.0052	0.515	48	0.962
		2D	5.24	0.0064	0.484	69	0.964
	50	3D	1.83	0.0098	0.464	16	0.964
		2D	4.71	0.0053	0.476	33	0.967

TABLE II. Results from 2D and 3D modeling with resist thickness varied from 400 to 500 nm and beam energy from 10 to 50 keV.

Thickness (nm)	Beam energy (keV)	3D/2D	Modeling error (nm/layer)	σ_0	α	x_t (nm)	b
400	10	3D	0.84	0.0140	0.506	77	0.987
		2D	28.90	0.0153	0.471	31	0.960
	20	3D	0.71	0.0115	0.524	41	0.975
		2D	15.98	0.0105	0.553	31	0.960
	30	3D	0.31	0.0093	0.482	56	0.960
		2D	10.66	0.0255	0.523	55	0.961
	40	3D	1.19	0.0098	0.437	33	0.965
		2D	8.33	0.0086	0.502	45	0.966
	50	3D	0.53	0.0046	0.573	51	0.987
		2D	6.40	0.0059	0.532	60	0.966
500	10	3D	6.25	0.0167	0.494	76	0.966
		2D	41.03	0.0161	0.514	77	0.967
	20	3D	1.27	0.0128	0.455	32	0.960
		2D	24.29	0.0163	0.464	29	0.968
	30	3D	0.64	0.0121	0.552	61	0.964
		2D	15.66	0.0085	0.560	40	0.967
	40	3D	4.26	0.0102	0.474	18	0.962
		2D	11.60	0.0188	0.471	96	0.979
	50	3D	2.03	0.0089	0.539	95	0.969
		2D	10.54	0.0082	0.515	66	0.984

TABLE III. Estimation of the CD and LER through the PEC based on the 2D and 3D modeling results for the resist thickness of 100 nm and the target CDs of 40 nm and 70 nm.

Target width (nm)	Beam energy (keV)	ΔW (nm)		Optimal dose		CD error (nm)		LER (nm)	
		3D	2D	3D	2D	3D	2D	3D	2D
40	10	3	3	0.438	0.414	−0.17	−1.96	0.31	0.49
	20	3	2	0.825	0.731	−0.40	−1.00	0.20	0.49
	30	2	2	1.063	1.047	−0.03	−0.40	0.23	0.30
	40	2	2	1.190	1.167	0.05	−0.36	0.20	0.27
	50	2	2	1.375	1.383	−0.42	−0.27	0.27	0.24
70	10	3	3	0.432	0.403	−0.01	−2.48	0.35	0.63
	20	3	2	0.820	0.726	−0.36	−1.22	0.19	0.55
	30	2	2	1.061	1.047	−0.05	−0.38	0.24	0.30
	40	2	2	1.195	1.168	0.16	−0.29	0.20	0.27
	50	2	2	1.392	1.379	−0.11	−0.31	0.21	0.25

Published under license by AVS.

IV. VERIFICATION

The accuracy of the 3D modeling is further verified through the proximity effect correction with the modeled LSF and noise.

A. Width reduction

In this study, for the correction of the proximity effect, the width of a feature to be exposed is reduced from the target width W by $2\Delta W$, where ΔW is the width reduction on each side of the feature as illustrated in Fig. 9, and the dose to be given to the reduced feature width is computed such that the CD error is minimized through an iterative procedure shown in Fig. 10.

When the CD error is minimized with $2\Delta W > 0$, the boundary of a written feature would be outside the exposed area. The LER tends to be much smaller outside than inside an exposed area. This is due to the fact that the exposure level is lower and the absolute fluctuation of exposure is smaller in the unexposed area. Therefore, the reduction of feature width helps achieving a smaller LER.

A proper ΔW can be larger for a broader LSF, i.e., proportional to the standard deviation of the fitted LSF from modeling. However, the width reduction also decreases the exposure contrast over the feature boundary, which is not desirable from the viewpoint of process stability. Also, when ΔW is too large, an impractically high dose would be required or the feature may not be developed to its full width. Hence, an upper limit of ΔW is necessary, and the ΔW is determined empirically as follows:

$$\Delta W = \min\left\{\lfloor 2\sigma_l + \frac{1}{2}\rfloor, 7\right\},$$

where σ_l is the standard deviation of the fitted main lobe of the modeled deterministic LSF.

B. Dose correction

With the reduced width of a feature, the optimal dose that minimizes the CD error is derived iteratively using a bisection procedure. In this derivation, the modeled deterministic LSF and noise are employed. The CD error is defined as the difference between the target CD and the average CD on the top and bottom layers.

In this study, the 3D modeling is carried out for reference cases for which the stochastic LSFs are known (generated through a Monte Carlo simulation). In each case, the optimal dose is used with the respective stochastic LSF to compute the exposure distribution and obtain the CD and LER following the development simulation.[13]

TABLE IV. Estimation of the CD and LER through the PEC based on the 2D and 3D modeling results for the resist thickness of 200 nm and the target CDs of 40 nm and 70 nm.

Target width (nm)	Beam energy (keV)	ΔW (nm)		Optimal dose		CD error (nm)		LER (nm)	
		3D	2D	3D	2D	3D	2D	3D	2D
40	10	6	6	0.839	0.743	0.81	−7.94	0.34	0.80
	20	4	4	1.330	1.209	0.36	−4.79	0.21	0.68
	30	4	3	1.854	1.690	−0.75	−2.51	0.15	0.50
	40	3	3	1.979	1.871	0.09	−1.82	0.14	0.31
	50	2	3	2.203	2.246	0.01	−1.15	0.30	0.17
70	10	6	6	0.727	0.702	−2.75	−5.69	0.49	0.65
	20	4	4	1.275	1.195	−0.57	−4.54	0.26	0.68
	30	4	3	1.819	1.675	−1.07	−3.12	0.16	0.62
	40	3	3	1.950	1.861	−0.23	−2.05	0.15	0.35
	50	2	3	2.199	2.238	0.03	−1.18	0.31	0.19

TABLE V. Estimation of the CD and LER through the PEC in terms of the 2D and 3D modeling results for the resist thickness of 300 nm and the target CDs of 40 nm and 70 nm. "NA" indicates that the resist is not fully developed.

Target width (nm)	Beam energy (keV)	ΔW (nm)		Optimal dose		CD error (nm)		LER (nm)	
		3D	2D	3D	2D	3D	2D	3D	2D
40	10	7	7	1.328	1.078	2.44	−20.99	0.65	NA
	20	3	4	1.690	1.592	1.77	−10.34	0.55	NA
	30	4	3	2.328	2.213	−0.19	−2.40	0.31	0.76
	40	3	3	2.500	2.416	0.25	−3.22	0.28	0.88
	50	4	4	2.953	2.839	−1.27	−3.53	0.20	0.43
70	10	7	7	1.006	0.929	−0.96	−16.43	0.83	1.74
	20	3	4	1.583	1.553	−0.54	−5.83	0.76	1.21
	30	4	3	2.247	2.167	−1.24	−3.04	0.34	0.88
	40	3	3	2.462	2.387	−0.18	−4.05	0.29	0.99
	50	4	4	2.870	2.815	−2.30	−3.72	0.24	0.45

V. RESULTS AND DISCUSSION

A. Simulation

Reference resist profiles, for which the stochastic LSFs are known, are used in the modeling. Note that, for arbitrary SEM

TABLE VI. Estimation of the CD and LER through the PEC in terms of the 2D and 3D modeling results for the resist thickness of 400 nm and the target CDs of 40 nm and 70 nm. "NA" indicates that the resist is not fully developed.

Target width (nm)	Beam energy (keV)	ΔW (nm)		Optimal dose		CD error (nm)		LER (nm)	
		3D	2D	3D	2D	3D	2D	3D	2D
40	10	7	7	2.021	1.535	−0.01	−18.23	1.05	NA
	20	7	5	2.469	2.072	0.15	−20.07	0.49	NA
	30	4	6	2.846	2.795	−0.91	−17.45	0.47	NA
	40	3	4	3.065	2.952	1.73	−7.53	0.32	1.39
	50	4	3	3.555	3.378	−0.55	−6.24	0.26	1.51
70	10	7	7	1.357	1.196	0.32	−33.65	0.96	NA
	20	7	5	2.086	1.919	−0.17	−11.81	0.45	1.35
	30	4	6	2.715	2.665	−0.36	−7.79	0.42	0.72
	40	3	4	2.937	2.895	−0.16	−4.75	0.48	0.83
	50	4	3	3.480	3.346	−0.76	−4.70	0.28	1.14

Published under license by AVS.

TABLE VII. Estimation of the CD and LER through the PEC in terms of the 2D and 3D modeling results for the resist thickness of 500 nm and the target CDs of 40 nm and 70 nm. "NA" indicates that the resist is not fully developed.

		ΔW (nm)		Optimal dose		CD error (nm)		LER (nm)	
Target width (nm)	Beam energy (keV)	3D	2D	3D	2D	3D	2D	3D	2D
40	10	7	7	2.859	1.534	−12.96	−16.61	NA	NA
	20	7	7	3.282	2.959	3.14	−20.29	0.54	NA
	30	6	5	3.651	3.258	−1.98	−20.20	0.57	NA
	40	6	6	3.906	3.578	1.69	−5.57	0.29	NA
	50	3	5	4.097	4.031	1.13	−9.66	0.37	1.40
70	10	7	7	1.792	1.509	−5.32	−30.81	1.20	NA
	20	7	7	2.513	2.352	2.01	−15.30	0.54	1.46
	30	6	5	3.227	3.045	−0.28	−13.18	0.49	1.70
	40	6	6	3.475	3.353	−1.83	−7.75	0.40	0.94
	50	3	5	3.916	3.873	−1.04	−9.50	0.60	1.19

images, the (true) LSF is not known, and therefore, the accuracy of modeling cannot be analyzed. Each reference resist profile is obtained from the respective stochastic LSF obtained from a Monte Carlo simulation for the substrate system consisting of PMMA on Si. To analyze the versatility of the 3D modeling, a number of reference resist profiles are generated by varying lithographic and feature parameters. The beam energy is varied from 10 to 50 keV, the resist thickness from 100 to 500 nm, the feature (line) width from 20 to 120 nm, and 4 different dose levels are employed for each feature width.

The features with widths of 20, 60, and 120 nm are employed in the modeling and 40 and 70 nm for the verification. The pixel sizes for exposure calculation and development simulation are 1 nm and 0.1 nm, respectively.

B. Modeling

The modeled deterministic LSFs are provided for varying resist thickness and beam energy in Fig. 11 where each LSF is normalized by its total energy (exposure). It can be seen that the shape of LSF follows the expected general trend. The LSF is sharper for a higher beam energy or a thinner resist. When the beam energy is higher, electrons are scattered less in the lateral direction and deposit their energy mostly in a small area, leading to a sharper LSF. In the case of a thinner resist, electrons still maintain a relatively higher energy when they arrive at the substrate interface; i.e., there is a smaller (vertical) space through which they can be scattered and therefore, they have been scattered less reaching the interface. This results in a sharper LSF. It is also observed that there is a smaller difference in the shape of LSF among different levels of beam energy when the resist is thinner but a larger difference for a thicker resist. These can be understood through the same reasoning.

The accuracy of modeling has been analyzed in detail, and the analysis results, i.e., average modeling error (cost function), are provided in Tables I and II. From the tables, it is seen that the modeling error is much smaller for the 3D modeling than for the 2D modeling. Also, the modeling error tends to become significantly larger as the resist thickness increases in the case of 2D modeling while it remains to be small. This well justifies the need to use the proposed 3D modeling compared to the 2D modeling.

C. Verification

The results from the dose correction, i.e., the CD error and LER, are provided in Tables III–VII. As in the modeling, various thicknesses of resist and levels of beam energy are considered. Overall, it is seen that the CD error and LER achieved by the 3D model are significantly smaller than those by the 2D model. The improvement by the 3D model is larger when the resist is thicker or the beam energy is lower. These are the cases where the exposure distribution varies more with the resist layer, and therefore, the 3D model can describe the exposure distribution in the resist more accurately. Note that the 2D model does not take into account the layer-dependent exposure variation.

The optimal dose computed using the 2D model is lower than that using the 3D model as can be seen in the tables. This makes the resist underdeveloped, especially at the bottom layer, leading a negative CD error. In the cases where the resist is thick and the beam energy is low, it can happen that the bottom layer is not developed at all, especially for a narrow feature. For a narrower feature, the exposure distribution is more layer-dependent. In such a case, the LER cannot be evaluated properly from the remaining resist profile (see "NA" in Tables V–VII). This occurs in 11 cases of the 2D results compared to only one case of the 3D results.

These verification results further confirm the advantages of and the need for the 3D modeling.

VI. SUMMARY

Modeling the e-beam lithographic process based on the information extracted from SEM images is a practical approach that has a potential to achieve high accuracy in the CD estimation and correction. The 2D modeling approach previously developed does not consider the exposure variation along the depth dimension of resist. This can result in lower accuracy when the resist is thicker or the beam energy is lower. Hence, in this study, a 3D approach to the modeling has been investigated in order to develop a more general modeling approach. The layer dependency of exposure is expressed by the layer ratio with the LSF of the middle layer directly modeled. The iterative modeling process adopts the simulated annealing to enhance the possibility of finding a good quality

Published under license by AVS.

solution (model). Through an extensive simulation, the 3D modeling has been tested for various combinations of resist thickness and beam energy. The modeling errors (CD and LER) are substantially smaller than those by the 2D modeling in most cases, and the shape of modeled LSF shows an expected dependency on the resist thickness and beam energy. Also, the proximity effect correction has been performed on L/S patterns using the modeled LSF including the noise for further verification. In terms of the CD error and LER achieved through the proximity effect correction, the 3D modeling is shown to have a clear advantage over the 2D modeling. Therefore, it may be said that the 3D modeling approach has a good possibility of being developed into a useful tool for estimating the CD and LER.

ACKNOWLEDGMENT

This work was supported by a research grant from Samsung Electronics Co., Ltd.

DATA AVAILABILITY

The data that support the findings of this study are available within the article.

REFERENCES

[1]F. Hu and S.-Y. Lee, J. Vac. Sci. Technol. B **21**, 2672 (2003).
[2]Q. Dai, S.-Y. Lee, S.-H. Lee, B.-G. Kim, and H.-K. Cho, J. Vac. Sci. Technol. B **29**, 06F314 (2011).
[3]G. P. Watson, L. A. Fetter, and J. A. Liddle, J. Vac. Sci. Technol. B **15**, 2309 (1997).
[4]R. Rau, J. McClellan, and T. Drabik, J. Vac. Sci. Technol. B **14**, 2445 (1996).
[5]M. J. Burek and J. R. Greer, Nano Lett. **10**, 69 (2010).
[6]R. Murali, D. Brown, K. Martin, and J. Meindl, J. Vac. Sci. Technol. B **24**, 2936 (2006).
[7]S.-Y. Lee and B. D. Cook, IEEE Trans. Semicond. Manuf. **11**, 108 (1998).
[8]G. P. Patsis, N. Tsikrikas, D. Drygiannakis, and I. Raptis, Microelectron. Eng. **87**, 1575 (2010).
[9]Z. Yu, L. Chen, W. Wu, H. Ge, and S. Y. Chou, J. Vac. Sci. Technol. B **21**, 2089 (2003).
[10]Y. Ma, G. Tsvid, and F. Cerrina, J. Vac. Sci. Technol. B **21**, 3124 (2003).
[11]R. Guo, S.-Y. Lee, J. Choi, S.-H. Lee, I.-K. Shin, C.-U. Jeon, B.-G. Kim, and H.-K. Cho, J. Vac. Sci. Technol. B **31**, 06F408 (2013).
[12]R. Guo, S.-Y. Lee, J. Choi, S.-H. Park, I.-K. Shin, and C.-U. Jeon, J. Vac. Sci. Technol. B **34**, 011601 (2016).
[13]Q. Dai, R. Guo, S.-Y. Lee, J. Choi, S.-H. Lee, I.-K. Shin, C.-U. Jeon, B.-G. Kim, and H.-K. Cho, Microelectron. Eng. **127**, 86 (2014).
[14]D. Drouin, A. R. Couture, D. Joly, X. Tastet, V. Aimez, and R. Gauvin, Scanning **29**, 92 (2007).

Published under license by AVS.